Title

A fiber optic photoacoustic sensor for real-time heparin monitoring

Authors

Zhou, Jingcheng
Yim, Wonjun
Zhou, Jiajing
et al.

Publication Date

2022

DOI

10.1016/j.bios.2021.113692

Peer reviewed

HHS Public Access

Author manuscript

Biosens Bioelectron. Author manuscript; available in PMC 2023 January 15.

Published in final edited form as:

Biosens Bioelectron. 2022 January 15; 196: 113692. doi:10.1016/j.bios.2021.113692.

A fiber optic photoacoustic sensor for real-time heparin monitoring

Jingcheng Zhou[a], **Wonjun Yim**[b], **Jiajing Zhou**[a], **Zhicheng Jin**[a], **Ming Xu**[a], **Yash Mantri**[d], **Tengyu He**[b], **Yong Cheng**[a], **Lei Fu**[a], **Zhuohong Wu**[a], **Tiffany Hancock**[e], **William Penny**[e], **Jesse V. Jokerst**[a,b,c,*]

[a]Department of NanoEngineering, University of California, San Diego, 9500 Gilman Drive, La Jolla, CA, 92093, USA

[b]Materials Science and Engineering Program, University of California, San Diego, 9500 Gilman Drive, La Jolla, CA, 92093, USA

[c]Department of Radiology, University of California, San Diego, 9500 Gilman Drive, La Jolla, CA, 92093, USA

[d]Department of Bioengineering, University of California, San Diego, 9500 Gilman Drive, La Jolla, CA, 92093, USA

[e]Division of Cardiology, VA Healthcare System, San Diego, CA, 92161, USA

Abstract

Heparin is a common anticoagulant, but heparin overdose is a common intensive care unit (ICU) medication error due to the narrow therapeutic window of heparin. Conventional methods to monitoring heparin suffer from long turnaround time, the need for skilled personnel, and low frequency of sampling. To overcome these issues, we describe here a fiber optic photoacoustic (PA) sensor for real-time heparin monitoring. The proposed sensor was validated with *in vitro* testing and in a simulated *in vivo* model using the following samples: (1) phosphate-buffered saline (PBS), (2) spiked human plasma, (3) spiked whole human blood, and (4) clinical samples

*Corresponding author. Department of Nano Engineering, University of California, San Diego, 9500 Gilman Drive, La Jolla, CA, 92093, USA. jjokerst@ucsd.edu (J.V. Jokerst).

Author contributions

Jingcheng Zhou designed, fabricated and built the fiber optic PA sensor, performed experiments and wrote the original draft. Wonjun Yim helped the experiments. Jiajing Zhou, Zhicheng Jin, Ming Xu contributed on the figure's preparation. Yash Mantri helped processing of clinical samples. Tengyu He, Yong Cheng, Lei Fu and Zhuohong Wu contributed to visualization and data presentation. Tiffany Hancock collected the clinical samples from patients during cardiac procedures along with William Penny, who also provided manuscript revision. Jesse V. Jokerst designed experiments, wrote the original draft, and edited the final manuscript.

CRediT authorship contribution statement

Jingcheng Zhou: Conceptualization, Methodology, Software, Validation, Visualization, Writing – original draft. **Wonjun Yim:** Visualization, Investigation. **Jiajing Zhou:** Visualization. **Zhicheng Jin:** Visualization, Software. **Ming Xu:** Visualization. **Yash Mantri:** Investigation. **Tengyu He:** Visualization. **Yong Cheng:** Visualization. **Lei Fu:** Visualization. **Zhuohong Wu:** Visualization. **Tiffany Hancock:** Investigation. **William Penny:** Supervision, Writing – review & editing. **Jesse V. Jokerst:** Supervision, Writing – review & editing.

Declaration of competing interest

The authors declare that they have no known competing financial interests or personal relationships that could have appeared to influence the work reported in this paper.

Appendix A. Supplementary data

Supplementary data to this article can be found online at https://doi.org/10.1016/j.bios.2021.113692.

from patients treated with heparin. Samples were validated by comparing the PA signal to the activated partial thromboplastin time (aPTT) as well as the activated clotting time (ACT). Importantly, the proposed sensor has a short turnaround time (3 min) and a limit of detection of 0.18 U/ml in whole human blood. The PA signal is linear with heparin dose and correlates with the aPTT value (Pearson's r = 0.99). The PA signal from 32 clinical samples collected from eight patients linearly correlated with ACT values (Pearson's r = 0.89, *in vitro*; Pearson's r = 0.93, simulated *in vivo*). The PA signal was also validated against the cumulative heparin dose (Pearson's r = 0.94, *in vitro*; Pearson's r = 0.96, simulated *in vivo*). This approach could have applications in both *in vitro* and real-time *in vivo* heparin monitoring.

Keywords

Fiber optic sensor; Heparin monitoring; Photoacoustic imaging; Anticoagulation therapy

1. Introduction

Heparin is a highly sulfated and negatively charged glycosaminoglycan that can increases the activity of antithrombin 1000-fold to inactivate the clotting factors thrombin and Factor Xa (Rosenberg, 1985). Heparin has been widely used as an anticoagulant drug in surgical and cardiovascular medicine because of its short half-life, reversibility, and low cost (Hirsh et al., 2001). More than 500 million doses of heparin are used worldwide each year (Lindahl et al., 1994).

However, heparin overdose is a common intensive care unit (ICU) medication error due to its narrow therapeutic window (Kane-Gill et al., 2010); heparin overdose can cause hemorrhage or thrombocytopenia (Yuan et al., 2020). Therefore, heparin monitoring during therapy is crucial. Coagulation-based methods to heparin monitoring use peripheral blood samples and are the current gold standards: activated partial thromboplastin time (aPTT), anti-Xa analysis, thromboelastography (TEG), and activated clotting time (ACT). The aPTT has been the primary laboratory test used to monitor heparin, but it suffers long turn around times and a variable reference range. The aPTT is affected by variations in sample volume and diurnal changes (Vandiver and Vondracek, 2012). Anti-Xa analysis is not affected by underfilled collection tubes and is not impacted by variations in factor VIII or fibrinogen. However, extensive sample processing (1 h) is required to avoid heparin neutralization from platelet factor 4, and anti-Xa analysis is more expensive than the aPTT (Vera-Aguilera et al., 2016). The TEG and ACT are established in the operating room but require skilled operators and complex sample preparation. Furthermore, these tools all require intermittent blood sampling, and thus are limited to periodic determinations. In contrast, a technique providing real-time monitoring of heparin anticoagulant therapy would thus be of great benefit to patient care. One way to solve this problem is use an *in vivo* imaging signal rather than *in vitro* laboratory diagnostics.

Direct detection of heparin is valuable in monitoring heparin-based therapy. Previous direct heparin testing methods include acoustic methods (Chen et al., 2017), electrochemistry (Qi et al., 2013), nuclear magnetic resonance (Groult et al., 2017), Raman scattering

spectroscopy (Ji et al., 2018), fluorometry (Li et al., 2017; Mehta et al., 2018; Xu et al., 2014), and colorimetric analysis (Qu et al., 2017). However, these methods have yet to be broadly deployed for clinical care. A recent study used surface plasmon resonance to measure heparin (Yuan et al., 2020) but not yet in whole human blood.

Photoacoustic (PA) imaging is a hybrid imaging modality that combines the advantages of optical and ultrasound imaging (Chen et al., 2019; Lao et al., 2008; Zhou and Jokerst, 2020). PA imaging can provide deeper imaging depth and higher spatial resolution than traditional optical imaging methods and can provide higher contrast between different tissues than ultrasound (Mantri and Jokerst, 2020; Wang and Hu, 2012). PAI transfers light energy to the measured object and converts the light energy into spatially-confined heat and thus thermoelastic expansion leading to acoustic pressure waves detected at the transducer (Jin et al., 2020; Xu et al., 2021; Yim et al., 2021; Zhou et al., 2019a). We previously showed that the addition of heparin to phenothiazine dyes decreases the absorbance of the sample due to dye–heparin aggregation leading to fewer dye molecules in solution; at the same time, the aggregation increases the PA intensity because the dye molecules in the dye–heparin aggregate have reduced degrees of freedom and poor heat transfer to solvent (Wang et al., 2018).

We previously reported a mechanism by which a free dye (methylene blue) produces a significant increase in photoacoustic signal in the presence of the heparin (Wang et al., 2016). Subsequently, we reported a cellulose-based sensor (Nile blue A) to detect the heparin concentration *in vitro* (Jeevarathinam et al., 2019). However, to fully utilize this technology, the sensing element must be embedded *in vivo* for real-time monitoring, i.e., the sensor would pass through an intravenous catheter. This work described here miniaturizes the sensor to the point that it could be placed inside of an adult human vein. This sensor is the first fiber optic-based assay for both *in vitro* and real-time *in vivo* heparin monitoring in whole blood. This design capitalizes on the small size, light weight, good reliability, flexibility, and limited electromagnetic interference of optical fibers (Guo et al., 2020; Zhou et al., 2019b).

2. Materials and methods

2.1. Materials

Nile blue A and polyethylene glycol (Mn 7,000–9,000) (Bioultra 8000) were purchased from Sigma Aldrich Inc. and used as received. Phosphate buffered saline was purchased from Quality Biological and used without further purification. Methanol was purchased from Fisher and used without further purification. Whatman No. 2 filter paper circles were purchased from GE Healthcare, U.K. A multi-mode optical fiber with core diameter of 400 μm were purchased from Thorlabs, USA. Miniature Heat-Shrink Tubing was purchased from McMaster-Carr, USA. Transpore tapes were purchased from 3M. Unfractionated heparin (1000 U/ml) was purchased from McKesson Corporation, USA. Polytetrafluoroethylene (PTFE) tubing was purchased from Agilent Technologies.

2.2. Preparation of cellulose-based dye layer

The cellulose-based dye layer was prepared in two steps: Whatman filter papers were impregnated with PEG first and then Nile blue dye. The concentrations of PEG and dye were optimized iteratively (Jeevarathinam et al., 2019). Whatman filter paper was immersed in 2% w/v PEG in methanol for 20 s, and then dried under ambient conditions for 5–10 min. The cellulose substrate impregnated with PEG was then immersed in a 2.72×10^{-4} M methanol solution of Nile Blue A for 20 s and dried under ambient conditions for 10 min. The Nile blue A-infused paper was cut into strips and used for further fiber optic PA sensor fabrication.

2.3. Fiber optic PA sensor fabrication

The top of the dye layer was covered with a porous film protective layer made by using 3M Transpore tape. This two-layer structure was then cut into 8 × 0.5 mm rectangular strips and two heat shrink tubes were then used to fix the rectangular two-layer strip on the sidewall of the 400 μm core optical fiber. The coating and cladding part of this 400 μm core optical fiber were removed with a fiber optic stripper and sandpaper in advance. This step introduces light into the sidewall of the optical fiber. In future designs, the light can be emitted from the sidewall of the optical fiber. The two heat shrink tubes were separately heated by the heat gun for 20 s under 140 °C.

2.4. PA in vitro study: PBS, human plasma, and whole human blood

The fiber optic PA sensor, the bare optical fiber, and the 3M Millipore tape with a graphite mark as an internal standard were fixed on a petri dish. A 90-mm-diameter plastic petri dish was used for PBS and human plasma measurements. A 50-mm-diameter glass petri dish was used for whole human blood studies. The bare optical fiber served as a negative control. A graphite mark served as a reference for any fluctuations in laser power. The petri dish was filled with 70 ml of PBS for PBS measurement; 50 ml human plasma (50% diluted human plasma) for human plasma measurement; and 15 ml whole human blood for whole human blood measurement. The PA transducer scanned the sensor, bare fiber, and graphite reference longitudinally. Heparin was added to the petri dish repeatedly (increase in working concentration of 0.25 U/ml). The PA images were acquired every minute as the heparin was added. The maximum measurement time window for each concentration was 5 min. The maximum heparin concentration was set as 3.5 U/ml because this is the upper range of standard clinical care (Smythe et al., 2016).

2.5. PA study using a simulated in vivo model PBS, human plasma, and whole human blood

A mini-pump (Mini-pump variable flow, Fisher Scientific), two flow tubes (PTFE Tubing, 1.75 mm diameter, Agilent), and two centrifuge tubes (Falcon Conical Centrifuge Tube, Fisher) (50 ml tube for PBS and human plasma; 15 ml tube for whole human blood) were used to establish a simulated human arm vein *in vivo* environment. The minipump was used to provide liquid flow at 1 ml/min. PTFE flow tubes were used to simulated human arm veins. Centrifuge tubes were used to contain incoming and outgoing flow liquids. The fiber optic PA sensor was inserted into the PTFE flow tube. The PTFE flow tube loaded with

the fiber optic PA sensor was arranged at the bottom of the water tank. The PA transducer scanned the flow tube with the fiber sensor inside and parallel to the direction of flow. PBS (50 ml), human plasma (50 ml 50% in PBS), or whole human blood (15 ml) were used as the fluid. Heparin was added to the centrifuge tube repeatedly (increase in working concentration of 0.5 U/ml). The PA images were obtained every minute when the heparin was added. The maximum heparin concentration was set as 3.5 U/ml.

2.6. Photoacoustic study in clinical samples

All human subject work was done with IRB approval from UCSD and the San Diego Veterans Administration Hospital. Thirty-two clinical samples were obtained from eight patients undergoing invasive clinical cardiac procedures in which a large dose of intravenous heparin for anticoagulation was administered. Four samples were collected from each patient at different time points during the heparin administration; one sample was collected at baseline before any heparin administration. The same samples had an ACT done at the time of collection. Plasma was centrifuged from clinical whole blood samples and stored at −80 °C. See details in Table S1.

We used 16 samples for *in vitro* measurements and 16 for the simulated *in vivo* model. (More details are described in the supplementary information section 1.1). For *in vitro* measurements, the fiber optic PA sensor, bare fiber and graphite marked reference tape were fixed on a petri dish (90 mm diameter plastic petri dish) and all treated with a 30-μ1 drop of plasma. Three minutes later, the petri dish with the heparin sensor and reference samples was rinsed twice with PBS and imaged longitudinally using 70 ml of PBS as a coupling media. For measurements using the *in vivo* model, the fiber optic PA sensor was fixed inside of a PTFE tube filled with PB S. The PTFE tube was fixed on a petri dish (90 mm diameter plastic petri dish) containing with 70 ml PBS. For each scan, the fiber optic PA sensor was pulled out from the PTFE tube and treated with 30 μl of plasma. Three minutes after each addition, the fiber optic PA sensor was rinsed twice with PBS, returned to the PTFE tube filled with PBS, and imaged through PBS.

3. Results and discussion

Heparin is a polysulfated glycosaminoglycan with a net negative charge that can bind with cationic dyes such as Nile blue A to change the absorbance spectra and PA intensity (Fig. 1a and Fig. S1). Here, we built a fiber optic PA sensor (Fig. 1b–e) for both *in vitro* and simulated *in vivo* measurements. The diameter of this fiber sensor is 850–900 μm. The structure and a photo of the fiber optic PA sensor are shown in Fig. 1b and d, respectively. The fiber optic PA sensor is built by an optical fiber, two heat shrinking tubes, a small size dye layer, and a porous film protective layer. The porous film protective layer protects the dye from detachment during blood flow. The proposed fiber optic PA sensor combines with the catheter for real-time heparin monitoring (Fig. 1c and e). The metal tip of the catheter is removed during the PA imaging experiment and does not affect PA signal.

3.1. Characterization of fiber optic PA sensor in PBS, human plasma, and whole human blood in vitro

The fiber optic PA sensor can respond to heparin via the formation of heparin-Nile blue A aggregates due to electrostatic interaction (Wang et al., 2018). The PA signal changes in the cellulose-based dye layer in PBS are detailed in Fig. S2. The fiber optic PA sensor was next studied in PBS, diluted plasma, and whole human blood *in vitro* (Fig. 2). PA images from the diluted plasma (50% human plasma) experiment are presented in Fig. 2a. The PA image of the fiber sensor was collected 5 min after addition of heparin. PA data for whole human blood experiments including the bare fiber and the reference graphite are presented in Fig. S3. Fig. 2b–d shows the relative PA intensity (PA intensity/reference graphite intensity) at different measurement time on different heparin concentration for PBS, diluted plasma, and whole human blood medium. The increase of PA intensity at different heparin concentrations reached equilibrium approximately 3 min after heparin was added indicating the stability of this fiber optic PA sensor. Note that the graphite was included as an internal control to compensate for differences in laser intensity.

The comparison between heparin concentration and PA intensity for PBS, diluted plasma, and whole human blood are shown in Fig. 2e and Fig. S3. The PA of the heparin sensor increased, but the PA of the reference graphite did not change during the test, which indicates that the increased PA signal comes from heparin not hemoglobin or deoxyhemoglobin in whole blood, although these heme-containing species definitely increase the background. Pearson's linear correlation coefficient of sensor PA response between 0 and 2.0 U/ml heparin is 0.988 for PBS, 0.975 for diluted plasma, and 0.987 for whole blood. The slope in whole blood is 3.8-fold higher than PBS, and 1.8-fold higher than diluted plasma. The relative standard deviation was <9.9% in PBS, < 12.4% in diluted plasma, and <12.7% in whole blood. There is higher background with whole blood, but the signal from heparin is still detectable above this elevated background. Surprisingly, the slope of the response is even sharper in whole blood. Future work will evaluate spectral deconvolution techniques to further refine the detection limits.

Therapeutic heparin levels vary widely but are usually higher than 0.25 U/ml: thromboembolism (7–8 U/ml), acute myocardial infarction (2.5 U/ml), coronary angioplasty (2.0 U/ml), extracorporeal circulation (5.6 U/ml), and extracorporeal membrane oxygenation (0.5 U/ml) (Wang et al., 2018). The detection limits of our sensor are 0.17 U/ml in PBS, 0.25 U/ml in diluted plasma, and 0.18 U/ml in whole blood. Therefore, the sensing window of our sensor is within the clinical-relevant ranges of heparin; of course, sample dilution could also be used.

3.2. Characterization of fiber optic PA sensor in PBS, human plasma and whole human blood in a simulated in vivo model

The fiber optic PA sensor has also been studied in PBS, diluted plasma, and whole human blood in a simulated *in vivo* model. The model measurement setup is shown in Fig. 3a and Fig. S4. The details of this setup have been discussed in section 2.2. The simulated *in vivo* system uses a flow rate of 1 ml/min because the blood flow rate in human arm veins is 1.2—4.8 ml/min (Klarhofer et al., 2001). The diameter of the tube is 1.75 mm, which is

comparable to a human arm vein (1.9–2.7 mm) (Spivack et al., 2012). the fiber optic PA sensor needs to be small enough to be placed into a human vein through a catheter without obstructing blood flow. Therefore, in the simulated *in vivo* model, we reduced the diameter of the tube (1.75 mm) to be even smaller than that of a normal human arm vein (1.9–2.7 mm) to evaluate the limitations of the sensor. The flow rate and tube diameter are positively correlated, and thus we slightly reduced the flow rate in the simulated *in vivo* model versus normal physiology. It is unlikely that this minor difference will impact the performance.

Fig. 3b shows a side view of the PA and ultrasound image in the diluted plasma medium at different heparin concentrations. Fig. 3c shows the top view of the PA image in the same diluted plasma medium. Fig. 3d–f shows the PA intensity at different measurement times on different heparin concentrations for PBS, diluted plasma, and whole blood. The increase in the PA intensity at different heparin concentrations saturated approximately 3 min after heparin was added and remained stable.

The comparison between heparin concentration and PA intensity for PBS, diluted plasma, and whole blood medium for simulated *in vivo* measurements are shown in Fig. 3g and Fig. S4. Pearson's linear correlation coefficient of the sensor's PA response between 0 and 2.0 U/ml heparin is 0.996 for PBS, for 0.993 for diluted plasma, and 0.994 for whole blood. The slope in whole blood is 2.5-fold higher than PBS, and 45% higher than diluted plasma (Fig. S4c). The relative standard deviation was <12.2% in PBS, < 15.4% in diluted plasma, and <16.6% in whole blood. The limit of detection is 0.15 U/ml in PBS, 0.21 U/ml in diluted plasma, and 0.19 U/ml in whole blood. There is a slight difference between the simulated *in vivo* data and the *in vitro* data, which may be caused by attenuation of the PA signal from the PTFE tube and/or the flow rate of the medium in the tubing. Nevertheless, these results show that the fiber optic PA sensor could also be applied for real-time heparin measurement *in vivo* in the future.

Blood contains hemoglobin and deoxyhemoglobin that can also produce PA signal. It also contains various charged species that could also interact with the charged dye. Indeed, the mechanism of interaction between heparin and the dye in our system is electrostatic, and thus there is the potential for non-specific signal activation. Thus, we validated the fiber optic PA sensor in PBS, diluted plasma, and whole human blood sample. While there was an elevated PA signal (higher background) in whole human blood, the addition of heparin increased this signal even further. This was seen both in the *in vitro* experiments and simulated *in vivo* conditions (Figs. 2e and 3g). There are few matrices more complicated in whole blood; thus, these whole blood experiments build confidence for this technique—especially since whole blood is the site to be sampled in final deployment of this technology.

3.3. Correlation of PA response of sensors with aPTT

The PA signal in whole human blood was compared to aPTT values. Fig. 4 compares the PA response to the aPTT of plasma from freshly collected whole human blood. Fig. 4a shows the PA response *in vitro* and Fig. 4b shows the PA response simulated *in vivo*. Both results have a high linear correlation (Pearson's r = 0.99). The PA response was between 0 and 1.0 U/ml heparin. These results suggest that the PA signal can monitor heparin activity analogously to the aPTT.

3.4. Heparin sensing in clinical samples

The *in vitro* results for 16 clinical samples are shown in Fig. 5a, Fig. 5c and 5e. Fig. 5a illustrates the relative PA intensity (PA intensity/reference graphite intensity) versus the ACT values; Fig. 5c plots the relative PA intensity versus the cumulative heparin values; Fig. 5e shows the ACT values versus the cumulative heparin dose (cumulative heparin units administered indicate the sum of bolus heparin and I.V heparin). These data show high linear correlation coefficients (PA *vs.* ACT, Pearson's r = 0.89; PA *vs.* cumulative heparin, Pearson's r = 0.94; ACT *vs.* cumulative heparin, Pearson's r = 0.93). The change in PA response with respect to the ACT values and cumulative heparin dose are significant ($P < 0.0001$). The simulated *in vivo* results for the 16 clinical samples are plotted in Fig. 5b, d, and Fig. 5f. Fig. 5b shows the PA intensity versus the ACT values; Fig. 5d shows the PA intensity versus the cumulative heparin values; Fig. 5f shows the ACT values versus the cumulative heparin dose. These data are significantly linearly correlated (PA *vs.* ACT, Pearson's r = 0.93; PA *vs.* cumulative heparin, Pearson's r = 0.96; ACT *vs.* cumulative heparin, Pearson's r = 0.97). The change in PA response with respect to the ACT values and cumulative heparin dose are significant ($P < 0.0001$). The fiber sensor PA images of one single patient under different samples are shown in Fig. S5 and Fig. S6.

The linearities of the simulated *in vivo* test data are higher than that of the *in vitro* test data, which may because attenuation of the PA intensity by the PTFE tube prevents the PA signal from prematurely saturating. Alternatively, the clinical samples used in the simulated *in vivo* model tests are more inherently correlated (ACT *vs.* cumulative heparin) than *in vitro* tests because the ACT was measured clinically. The correlation between ACT and cumulative heparin of samples used to simulated *in vivo* tests (Pearson's r = 0.97) is more linear than that of samples used to *in vitro* tests (Pearson's r = 0.93) (Fig. 5e–f). Variations in ACT include different baseline ACT values, choice of activator, presence of drugs such as aprotinin, and the instrument used (Perry et al., 2010). Our approach demonstrated a close correlation between the PA intensity of the sensor and the ACT (Pearson's r = 0.89, *in vitro*; Pearson's r = 0.93, *in vivo* simulation) suggesting that this approach can not only measure heparin concentration but also acts as a surrogate for anticoagulant activity.

Our system has advantages and limitations versus other systems. Other dye-based heparin detection methods are more selective but have not been studied in complex biological samples (Bromfield et al., 2013; Buee et al., 1991). The colorimetric determination of heparin is largely limited to plasma and buffer; whole blood is clearly more complicated (You et al., 2017). The aPTT is limited by its range of detection (0.3–0.7 U/ml), variation in reagents, and operating time (Lehman and Frank, 2009). The anti-Xa method can cause problems in the treatment of antithrombin deficiency, post-thrombolysis, hyperbilirubinemia, end-stage renal disease, and pregnancy (Vera-Aguilera et al., 2016). ACT is insensitive to coagulation abnormalities and platelet deficiency (Tran et al., 2012). These drawbacks are overcome by our design, where our fiber optic PA sensor can work in complex biological environment (whole human blood and clinical samples), has a large range of detection (0–3.5 U/ml), can quickly measures heparin activity (~3 min), and requires only a small amount of blood sample (~30 μL). More importantly, our approach could have utility for real-time *in vivo* heparin monitoring.

4. Conclusion

We prepared a fiber optic PA sensor and used the PA imaging signal to measure heparin in whole blood samples. Both *in vitro* and simulated *in vivo* measurements were performed to validate the sensor performance. PBS, human plasma, and whole blood were used in the tests and the PA response of the sensor correlated with the aPTT and ACT. The correlation of the cumulative heparin level with the PA response of clinical samples is comparable to that of ACT suggesting that this method is monitoring heparin activity (not just concentration). Future work with the sensor will include transmission of light through the developed optical fiber, which will improve imaging depth and spatial resolution as well as the use of low-cost LED-based PA instruments to replace laser-based PA equipment.

Supplementary Material

Refer to Web version on PubMed Central for supplementary material.

Acknowledgements

We acknowledge funding from DP2 HL137187 and infrastructure from S10 OD021821.

References

Bromfield SM, Barnard A, Posocco P, Fermeglia M, Pricl S, Smith DK, 2013. J. Am. Chem. Soc 135, 2911–2914. [PubMed: 23406254]

Buee L, Boyle NJ, Zhang L, Delacourte A, Fillit HM, 1991. Anal. Biochem 195, 238–242. [PubMed: 1750673]

Chen D, Song S, Ma J, Zhang Z, Wang P, Liu W, Guo Q, 2017. Biosens. Bioelectron 91, 465–471. [PubMed: 28068607]

Chen H, Agrawal S, Dangi A, Wible C, Osman M, Abune L, Jia H, Rossi R, Wang Y, Kothapalli SR, 2019. Sensors 19, 5470.

Groult H, Poupard N, Herranz F, Conforto E, Bridiau N, Sannier F, Bordenave S, Piot JM, Ruiz-Cabello J, Fruitier-Arnaudin I, Maugard T, 2017. Biomacromolecules 18, 3156–3167. [PubMed: 28850787]

Guo X, Wu N, Zhou J, Du C, Wang X, 2020. Opt Laser. Eng 127, 105962.

Hirsh J, Anand SS, Halperin JL, Fuster V, 2001. Circulation 103, 2994–3018. [PubMed: 11413093]

Jeevarathinam AS, Pai N, Huang K, Hariri A, Wang J, Bai Y, Wang L, Hancock T, Keys S, Penny W, Jokerst JV, 2019. Biosens. Bioelectron 126, 831–837. [PubMed: 30602265]

Ji W, Zhang X, Zhao J, Gao Y, Song W, Ozaki Y, 2018. Analyst 143, 1899–1905. [PubMed: 29561561]

Jin Z, Sugiyama Y, Zhang C, Palui G, Xin Y, Du L, Wang S, Dridi N, Mattoussi H, 2020. Chem. Mater 32, 7469–7483.

Kane-Gill SL, Jacobi J, Rothschild JM, 2010. Crit. Care Med 38, S83–S89. [PubMed: 20502179]

Klarhofer M, Csapo B, Balassy C, Szeles JC, Moser E, 2001. Magn. Reson. Med 45, 716–719. [PubMed: 11284002]

Lao Y, Xing D, Yang S, Xiang L, 2008. Phys. Med. Biol 53, 4203–4212. [PubMed: 18635896]

Lehman CM, Frank EL, 2009. Labmedicine 40, 47–51.

Li J, Cheng M, Li M, 2017. Analyst 142, 3733–3739. [PubMed: 28872172]

Lindahl U, Lidholt K, Spillmann D, Kjellen L, 1994. Thromb. Res 75, 1–32. [PubMed: 8073404]

Mantri Y, Jokerst JV, 2020. ACS Nano 14, 9408–9422. [PubMed: 32806027]

Mehta PK, Hwang G, Park J, Lee K, 2018. Anal. Chem 90, 11256–11264. [PubMed: 30149703]

Perry DJ, Fitzmaurice DA, Kitchen S, Mackie IJ, Mallett S, 2010. Br. J. Haematol 150, 501–514. [PubMed: 20618331]

Qi H, Zhang L, Yang L, Yu P, Mao L, 2013. Anal. Chem 85, 3439–3445. [PubMed: 23445515]

Qu F, Liu Y, Lao H, Wang Y, You J, 2017. New J. Chem 41, 10592–10597.

Rosenberg RD, 1985. Fed. Proc 44, 404–409. [PubMed: 3155697]

Smythe MA, Priziola J, Dobesh PP, Wirth D, Cuker A, Wittkowsky AK, 2016. J. Thromb. Thrombolysis 41, 165–186. [PubMed: 26780745]

Spivack DE, Kelly P, Gaughan JP, van Bemmelen PS, 2012. Ultrasound Med. Biol 38, 190–194. [PubMed: 22230131]

Tran KM, Maxwell LG, Cohen DE, Adamson PC, Moll V, Kurth CD, Galinkin JL, 2012. Anesth. Analg 114, 1265–1267. [PubMed: 22025493]

Vandiver JW, Vondracek TG, 2012. Pharmacotherapy 32, 546–558. [PubMed: 22531940]

Vera-Aguilera J, Yousef H, Beltran-Melgarejo D, Teng T, Jan R, Mok M, Vera-Aguilera C, Moreno-Aguilera E, 2016. Adv. Hematol 4054806, 2016.

Wang J, Chen F, Arconada-Alvarez SJ, Hartanto J, Yap LP, Park R, Wang F, Vorobyova I, Dagliyan G, Conti PS, Jokerst JV, 2016. Nano Lett. 16, 6265–6271. [PubMed: 27668964]

Wang J, Jeevarathinam AS, Humphries K, Jhunjhunwala A, Chen F, Hariri A, Miller BR, Jokerst JV, 2018. Bioconjugate Chem. 29, 3768–3775.

Wang L, Hu S, 2012. Science 335, 1458–1462. [PubMed: 22442475]

Xu M, Yim W, Zhou J, Zhou J, Jin Z, Moore C, Borum R, Jorns A, Jokerst JV, 2021. IEEE Nanotechnol. Mag 15, 8–28.

Xu M, Yin C, Huo F, Zhang Y, Chao J, 2014. Sensor. Actuator. B Chem 204, 18–23.

Yim W, Zhou J, Mantri Y, Creyer MN, Moore CA, Jokerst JV, 2021. ACS Appl. Mater. Interfaces 13, 14974–14984. [PubMed: 33761255]

You J, Liu Y, Lu C, Tseng W, Yu C, 2017. Biosens. Bioelectron 92, 442–448. [PubMed: 27836604]

Yuan H, Ji W, Chu S, Liu Q, Guang J, Sun G, Zhang Y, Han X, Masson JF, Peng W, 2020. Biosens. Bioelectron 154, 112039. [PubMed: 32056956]

Zhou J, Guo X, Du C, Wang X, 2019a. Opt. Lett 44, 5390–5393. [PubMed: 31675015]

Zhou J, Jokerst JV, 2020. Photoacoustics 20, 100211. [PubMed: 33163358]

Zhou J, Wu N, Wang X, 2019b. Measurement 146, 668–674.

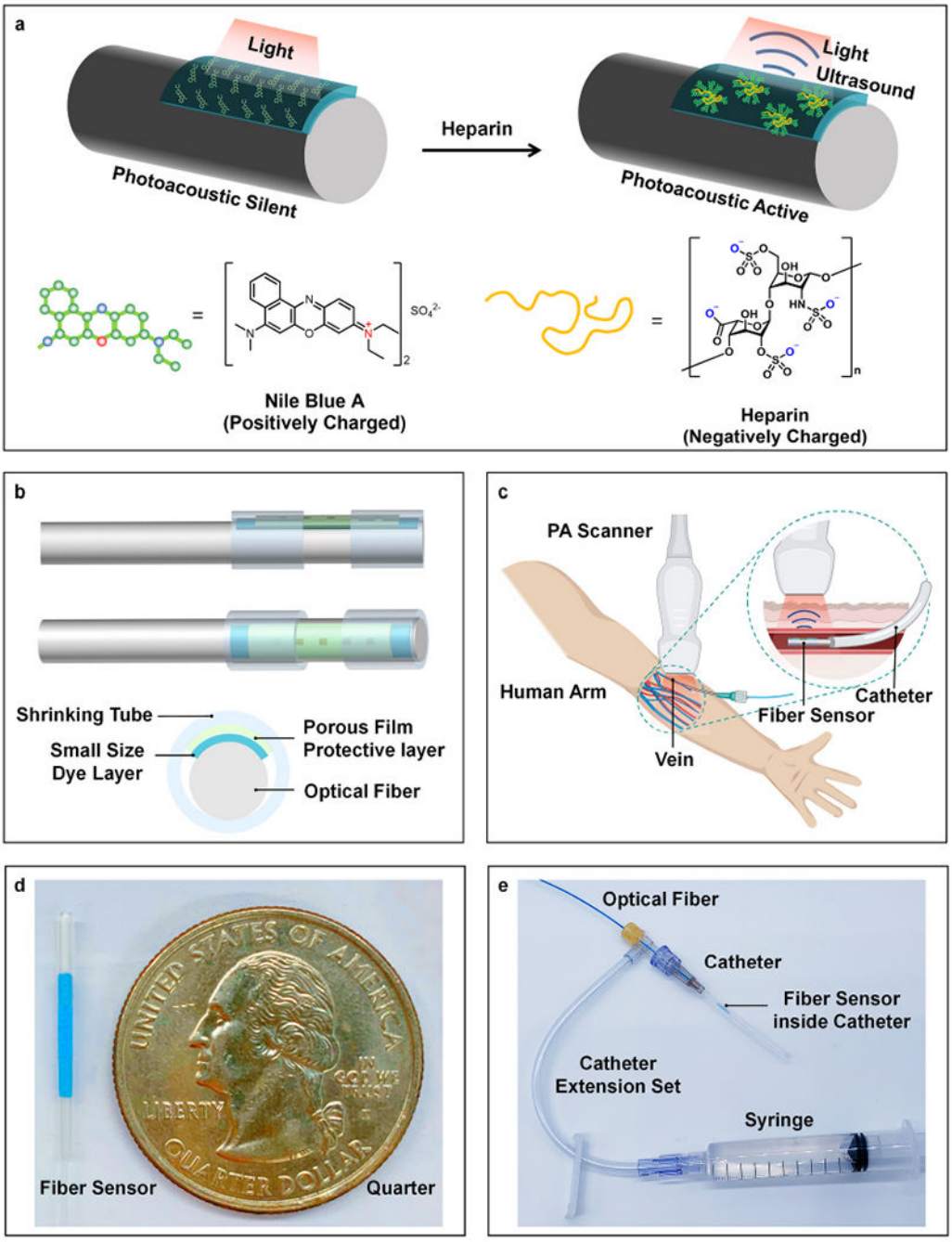

Fig. 1.

The structure of fiber optic PA sensor. a, Principle of fiber optic PA sensor: Cationic dyes with delocalized positive charges such as Nile Blue A can form aggregates with negatively charged heparin. Compared with non-aggregated Nile Blue A molecules, heparin-Nile Blue A aggregates have higher photoacoustic activity resulting in enhanced PA Signal. b, Fiber optic PA sensor structure: An optical fiber, two heat shrinking tubes, a small size dye layer, and a porous film protective layer constitute this fiber optic PA sensor. c, A schematic illustration of sensing mechanism of the sensors. The proposed fiber optic PA sensor is

inserted through a catheter, and the dye aggregated with heparin increases the PA signal on the fiber optic PA sensor. d, Photo of fiber optic PA sensor compared with a quarter. e, Photo of fiber optic PA sensor combined with the catheter. The fiber optic PA sensor is inserted through a catheter combined with a catheter extension set and a syringe. (For interpretation of the references to color in this figure legend, the reader is referred to the Web version of this article.)

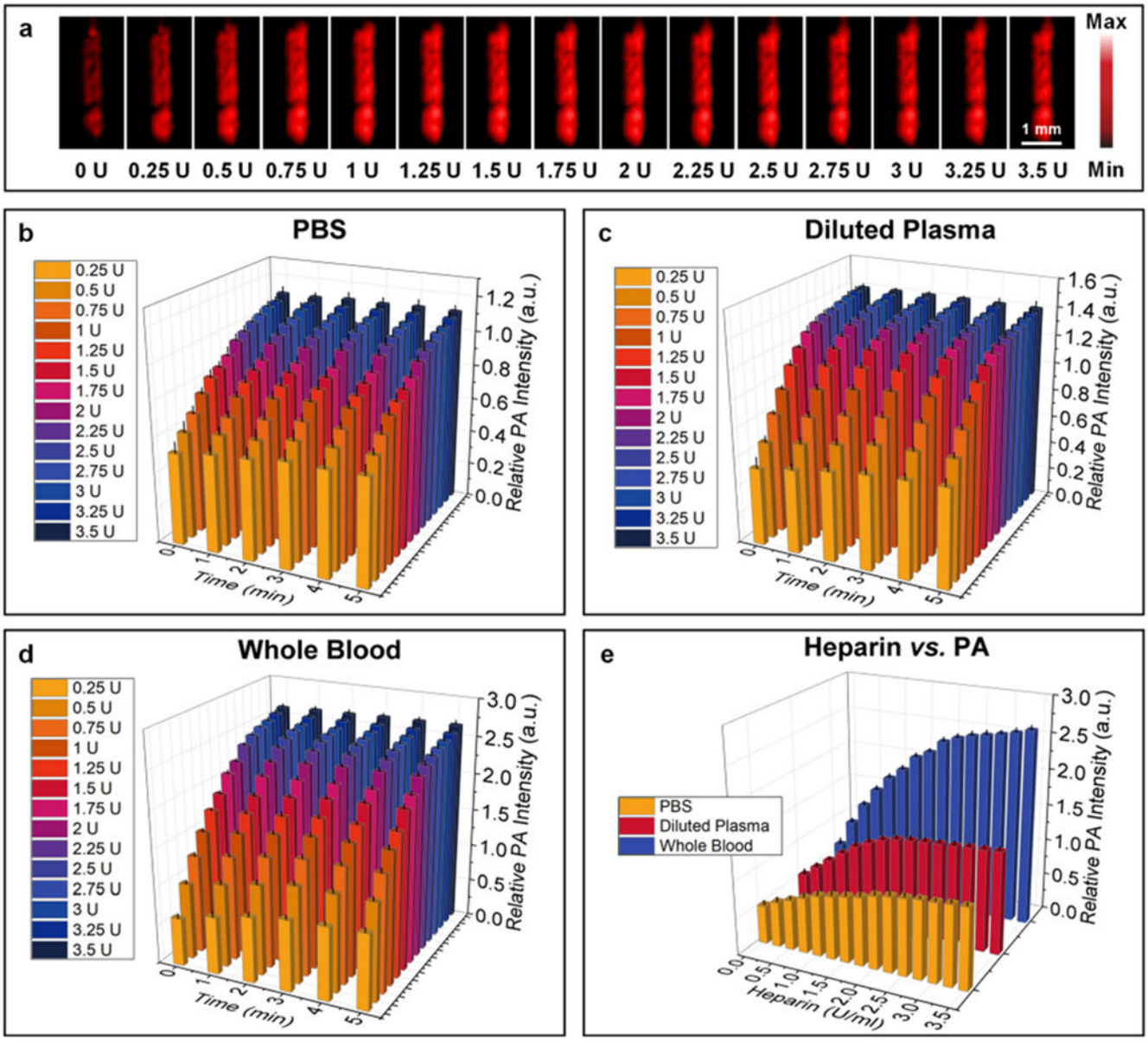

Fig. 2.

PA response of fiber optic PA sensor measured *in vitro* in PBS, diluted plasma and whole blood. a, PA images of the fiber optic PA sensor in diluted plasma at different heparin concentrations for *in vitro* measurement. The PA images were measured 5 min after heparin addition at each concentration. b, Relative PA intensity of fiber optic PA sensor in PBS *in vitro*. c, Relative PA intensity of fiber optic PA sensor in diluted plasma *in vitro*. d, Relative PA intensity of fiber optic PA sensor in whole blood *in vitro*. The increase of PA intensity at different heparin concentrations reached equilibrium approximately 3 min after heparin was added indicating the stability of this fiber optic PA sensor. e, Comparison between heparin concentration and relative PA intensity for PBS, diluted plasma and whole blood medium. The limit of detection is 0.17 U/ml in PBS, 0.25 U/ml in diluted plasma, and 0.18 U/ml in whole blood (0–2.0 U/ml). The relative standard deviation was <9.9% in PBS, <

12.4% in diluted plasma and <12.7% in whole blood. Error bars indicate the standard error corresponding to six different locations on the fiber optic PA sensor.

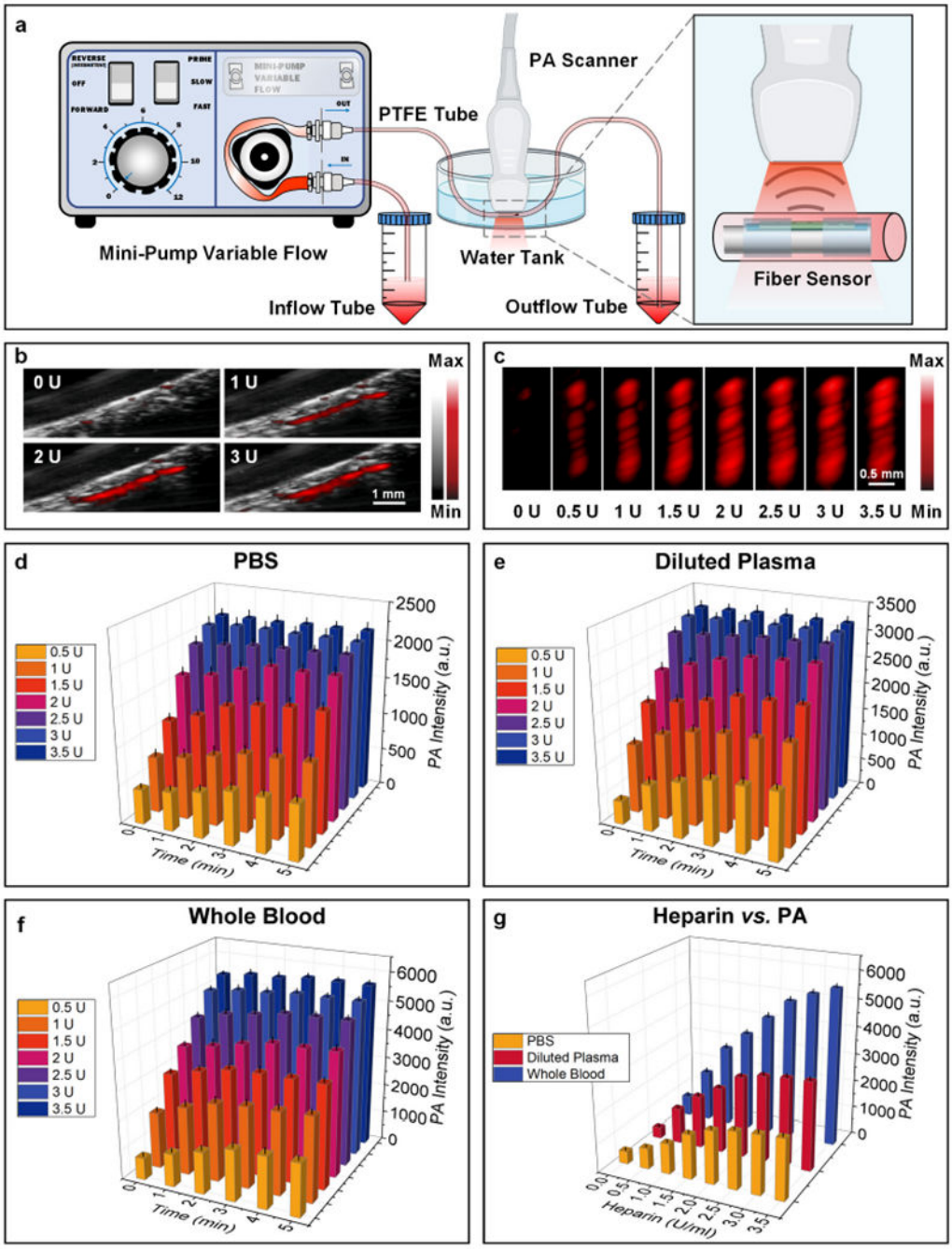

Fig. 3.

PA response of fiber optic PA sensor measured in a simulated *in vivo* environment in PBS, diluted plasma and whole blood. a, The simulated *in vivo* measurement setup. A mini-pump, two flow tubes (PTFE Tube, 1.75 mm diameter), and two centrifuge tubes were used to establish a simulated human arm vein *in vivo* environment. The side view (b) and top view (c) of the PA and ultrasound images are in diluted plasma medium at different heparin concentrations in the simulated *in vivo* model (a). The images were measured at the fifth minute of each concentration. PA intensity of the fiber optic heparin sensor in the simulated

in vivo model in PBS (d) diluted plasma (e), and whole blood (f). The increase of PA intensity at different heparin concentrations reached equilibrium approximately 3 min after heparin was added indicating the stability of this fiber optic PA sensor, g, Comparison between heparin concentration and PA intensity for PBS, diluted plasma, and whole blood medium in the simulated *in vivo* model. The limit of detection is 0.15 U/ml in PBS, 0.21 U/ml in diluted plasma, and 0.19 U/ml in whole blood (0–2.0 U/ml). The relative standard deviation was <9.9% in PBS, < 15.4% in diluted plasma, and <16.6% in whole blood. Error bars indicate the standard error corresponding to six different locations on the fiber optic PA sensor.

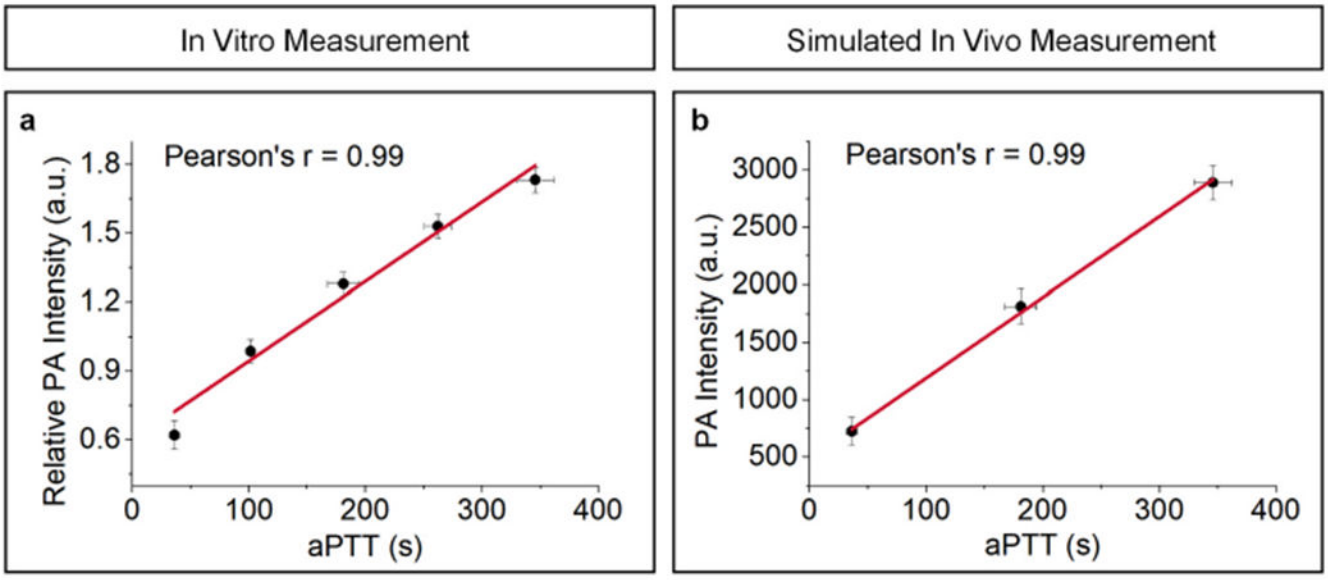

Fig. 4.

Correlation of aPTT and PA response of fiber optic PA sensor in whole blood. Linear correlation between the PA response of the sensor and aPTT values in whole human blood samples. a, *In vitro* measurements (Pearson's r = 0.99). b, Simulated *in vivo* measurements (Pearson's r = 0.99). The PA response was between 0 and 1.0 U/ml heparin. Error bars indicate the standard error corresponding to three times measurement of aPTT and six different locations on the fiber optic PA sensor.

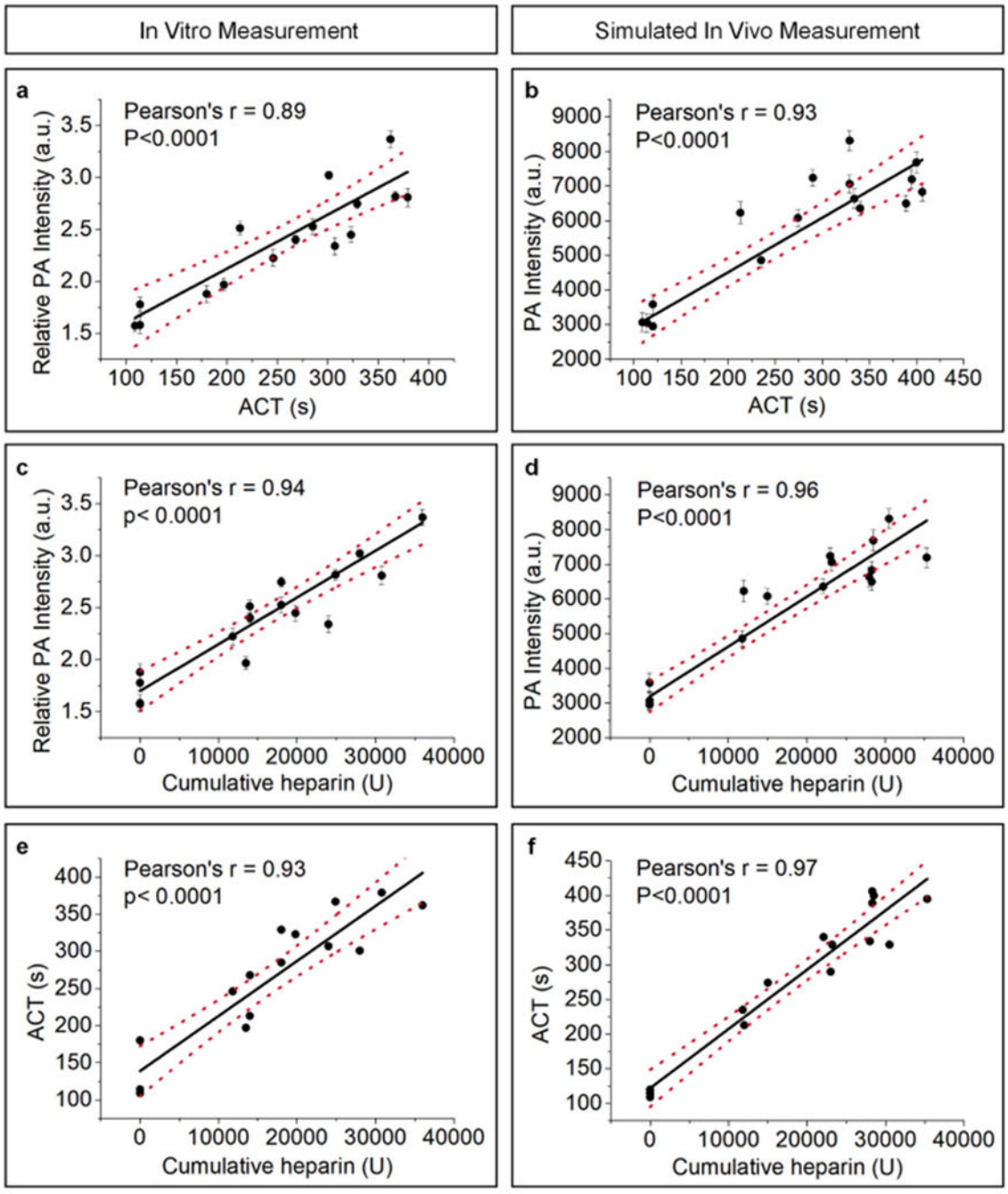

Fig. 5.

PA response of sensors to 32 clinical specimens collected from eight patients undergoing cardiac procedures requiring heparin. a, PA response versus ACT for *in vitro* measurements. b, PA response versus ACT for simulated *in vivo* measurements. c, PA response as a function of cumulative heparin dose for *in vitro* measurements. d, PA response as a function of cumulative heparin dose for simulated *in vivo* measurement. e, Linear correlation between ACT and cumulative heparin for *in vitro* measurement. f, Linear correlation between ACT

and cumulative heparin for simulated *in vivo* measurements. The dotted lines represent the 95% confidence interval band. Error bars in panels a, b, c, and d indicate the standard error.